Visualization of Gas Dynamics inside the Ion Funnel using Particle Tracking Velocimetry

Diamantis Kounadis[1]; Dimitris Papanastasiou[1]; Ioannis Orfanopoulos[1]; Alexander Lekkas[1]; Ioannis Nikolos[2]; Emmanuel Raptakis[1]

[1]Fasmatech, Athens, GR; [2]Department of Production Engineering & Management, TUC, Chania, Crete, GR

INTRODUCTION

The ion funnel is considered one of the important technological advancements in modern mass spectrometry with a significant impact on instrument sensitivity. Despite the extensive characterization of the device using experiments and ion optical simulations, very little is known on the gas dynamical properties of the device and their effect on ion transmission. Investigations based on ion optics simulation s/w have disregarded gas flow effects and a comprehensive study based on computational fluid dynamics has not yet been presented. Here, we present an experimental investigation of the gas dynamics inside the ion funnel using Particle Tracking Velocimetry (PTV).

METHODS

A prototype ion funnel assembly was designed using CAD software and constructed from a composite material using 3D color printing with a resolution of 300x450 dpi, which produced a model with accuracy of less than 0.1 mm. The thickness of the electrodes is 0.6 mm and an exit aperture of 2.5 mm is used. Inserts are constructed along the length of the funnel and sealed with glass windows, which allow for optical access with a laser and a CCD camera. The 3D model was introduced in the first vacuum compartment of a vacuum chamber equipped with a capillary inlet with 0.5 mm id. Tracer nanoparticles produced by high frequency spark discharges established between two graphite rods are used to seed the nitrogen flow pumped through the inlet capillary. Figure 1 (a) shows the two printed half-parts of the ion funnel and Figure 1 (b) shows the assembled model. Parts were painted black to reduce background noise on the CCD.

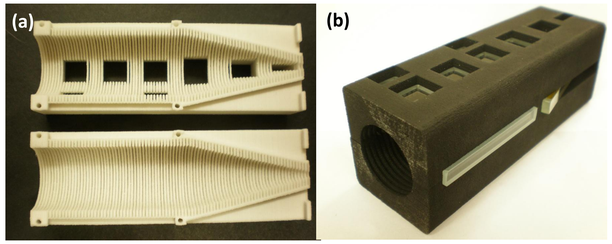

FIGURE 1. (a) Ion funnel model produced by 3D printing and (b) assembly showing glass ports for optical access.

The laser sheet is 1 mm thick and introduced through a 1 mm wide side slot running along the length of the funnel. An exit slot of equal length allows for the laser light to exit the device and eliminate light scattering on surfaces thus minimizing noise on the CCD. Laser light scattered on graphite nanoparticles is observed through optical ports with dimensions of 12x12 mm^2 near the entrance while smaller size ports are used toward the exit of the device. Alignment of the laser relative to the side slot is critical in order to avoid ablation of material which can form coagulates and produce unwanted signal on the CCD.

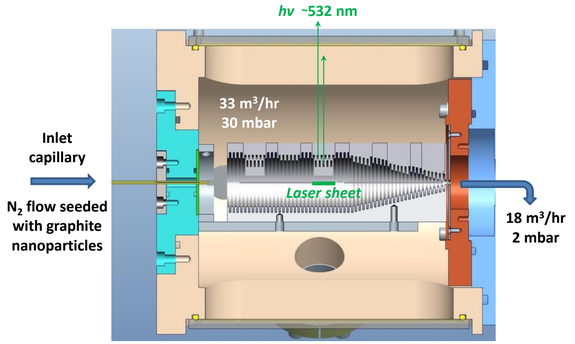

FIGURE 2. Cross section of the vacuum chamber showing inlet capillary, funnel and exit aperture to consecutive vacuum compartment.

The ion funnel is mounted on a supporting base and positioned 10 mm downstream from the outlet of the capillary interface. A 33 m^3/hr mechanical pump is used to evacuate the first vacuum compartment down to 30 mbar. The second vacuum compartment is operated at 2 mbar using a second mechanical pump. The aperture separating first and second vacuum regions is 2.5 mm and positioned 1 mm behind the end of the funnel. The inlet capillary is connected to the spark discharge source employed for the generation of carbonaceous nanoparticles. Both polydisperse and monodisperse particle distributions can be generated by controlling the current flowing into the discharge. The size distributions for the monodisperse particles is centered around 10 nm with a standard deviation of less than 3 nm, while the polydisperse particle distribution extends from a few nm up to 200 nm in size. Nitrogen is used as a carrier gas and delivered to the capillary at a flow rate of 0.9 L/min.

RESULTS

Velocity vector plots along the plane of the laser sheet are shown in the next Figures 3 and 4. The formation of the free jet remains undisturbed at the entrance of the funnel and image processing identifies particles with velocities exceeding 400 m/s, as shown in Figure 3 (a). Jet boundaries are confined to within ±2 mm during the first 20-30 mm. Further downstream the speed of the gas is reduced and the jet expands radially, as shown in Figure 3 (b). The diffusive nature of the jet near the breaking point is revealed in Figure 3 (c) where the recirculation zone overlaps with forward-moving particles extensively. Velocity profiles in the radial direction observed through the first three windows are shown in Figure 3 (d).

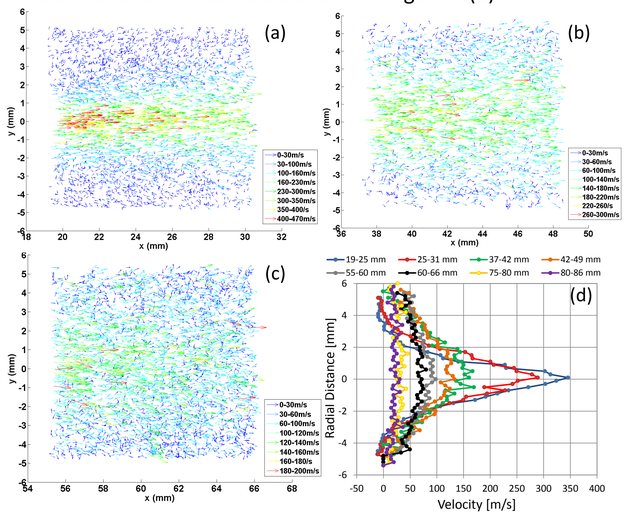

FIGURE 3. Velocity vectors determined by laser scattering of graphite nanoparticles as observed through the (a) first, (b) second and (c) third windows of the ion funnel. Velocity profiles in the radial direction (d) are also shown.

Velocity profiles at the entrance of the funnel show the region downstream from the Mach disk and the recirculation zone filled with slow particles moving in the opposite direction. As the speed of the gas reduces with distance and the boundaries of the jet expand radially the velocity profiles become quasi-parabolic after the first 55-60 mm from the entrance of the funnel. A flat profile is developed further downstream with a mean forward velocity of the order of 20-30 m/s.

In the second part of the funnel where electrode ID is progressively reduced the gas becomes highly diffusive and, despite the net forward motion of the flow, a significant fraction of the nanoparticles is moving backwards. The corresponding velocity vector field is shown in Figure 4 (a). Figure 4 (b) shows the vector field further downstream and the orderly structure of the diffusive gas in this region is revealed by plotting velocity and vector angle distributions shown in 4 (d). Finally, Figure 4 (c) shows the vector field near the exit of the funnel where nanoparticles undergo reacceleration as they move toward the flow-limiting end-aperture of the funnel. The velocity of the gas along the axis of the funnel is shown in Figure 5.

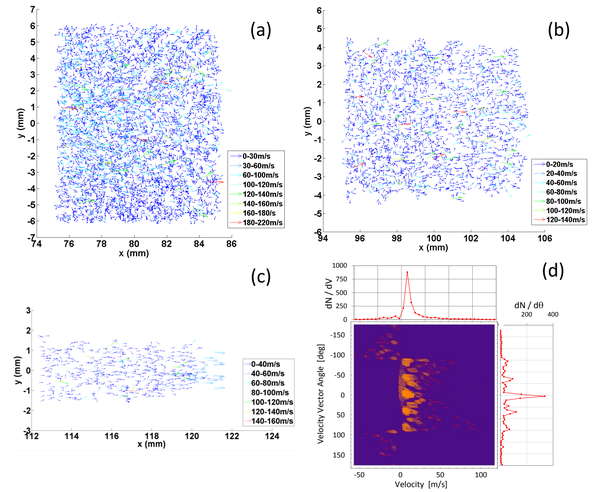

FIGURE 4. Velocity vector fields observed through the (a) fourth, (b) fifth and (c) sixth window of the ion funnel. Velocity and vector angle distributions for the fifth vector field are also shown in (d).

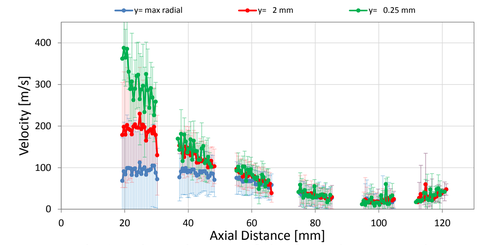

FIGURE 5. Velocity along the axis of the funnel integrated over different radial distances.